HHS Public Access

Author manuscript

Adv Funct Mater. Author manuscript; available in PMC 2020 June 26.

Published in final edited form as:

Adv Funct Mater. 2018 September 26; 28(39): . doi:10.1002/adfm.201801850.

3D Printed Stem-Cell Derived Neural Progenitors Generate Spinal Cord Scaffolds

Daeha Joung[*],
Department of Mechanical Engineering, University of Minnesota, Minneapolis, Minnesota 55455, USA

Vincent Truong[*],
Department of Neurosurgery, Stem Cell Institute, University of Minnesota, Minneapolis, Minnesota 55455, United States

Colin C. Neitzke,
Department of Neurosurgery, Stem Cell Institute, University of Minnesota, Minneapolis, Minnesota 55455, United States

Shuang-Zhuang Guo,
Department of Mechanical Engineering, University of Minnesota, Minneapolis, Minnesota 55455, USA

Patrick J. Walsh,
Department of Neurosurgery, Stem Cell Institute, University of Minnesota, Minneapolis, Minnesota 55455, United States

Joseph R. Monat,
Department of Mechanical Engineering, University of Minnesota, Minneapolis, Minnesota 55455, USA

Fanben Meng,
Department of Mechanical Engineering, University of Minnesota, Minneapolis, Minnesota 55455, USA

Sung Hyun Park,
Department of Mechanical Engineering, University of Minnesota, Minneapolis, Minnesota 55455, USA

James R. Dutton,
Stem Cell Institute, Department of Genetics, Cell Biology and Development, University of Minnesota, Minneapolis, Minnesota 55455, United States

Ann M. Parr[§],
Department of Neurosurgery, Stem Cell Institute, University of Minnesota, Minneapolis, Minnesota 55455, United States

[§]Corresponding authors mcalpine@umn.edu, amparr@umn.edu.
[*]D.J. and V.T. contributed equally to this work.

Supporting Information
Supporting Information is available from the Wiley Online Library or from the author.

Michael C. McAlpine[§]
Department of Mechanical Engineering, University of Minnesota, Minneapolis, Minnesota 55455, USA

Abstract

A bioengineered spinal cord is fabricated via extrusion-based multi-material 3D bioprinting, in which clusters of induced pluripotent stem cell (iPSC)-derived spinal neuronal progenitor cells (sNPCs) and oligodendrocyte progenitor cells (OPCs) are placed in precise positions within 3D printed biocompatible scaffolds during assembly. The location of a cluster of cells, of a single type or multiple types, is controlled using a point-dispensing printing method with a 200 μm center-to-center spacing within 150 μm wide channels. The bioprinted sNPCs differentiate and extend axons throughout microscale scaffold channels, and the activity of these neuronal networks is confirmed by physiological spontaneous calcium flux studies. Successful bioprinting of OPCs in combination with sNPCs demonstrates a multicellular neural tissue engineering approach, where the ability to direct the patterning and combination of transplanted neuronal and glial cells can be beneficial in rebuilding functional axonal connections across areas of central nervous system (CNS) tissue damage. This platform can be used to prepare novel biomimetic, hydrogel-based scaffolds modeling complex CNS tissue architecture *in vitro* and harnessed to develop new clinical approaches to treat neurological diseases, including spinal cord injury.

Abstract

A living platform to model spinal cord cytoarchitecture is introduced via 3D bioprinting, in which clusters of stem-cell derived spinal neuronal progenitor cells (sNPCs) and oligodendrocyte progenitor cells (OPCs) are placed in precise positions within biocompatible 3D printed scaffolds. The platform could ultimately be used as a therapeutic for chronic spinal cord injury to regenerate axons across the lesion site.

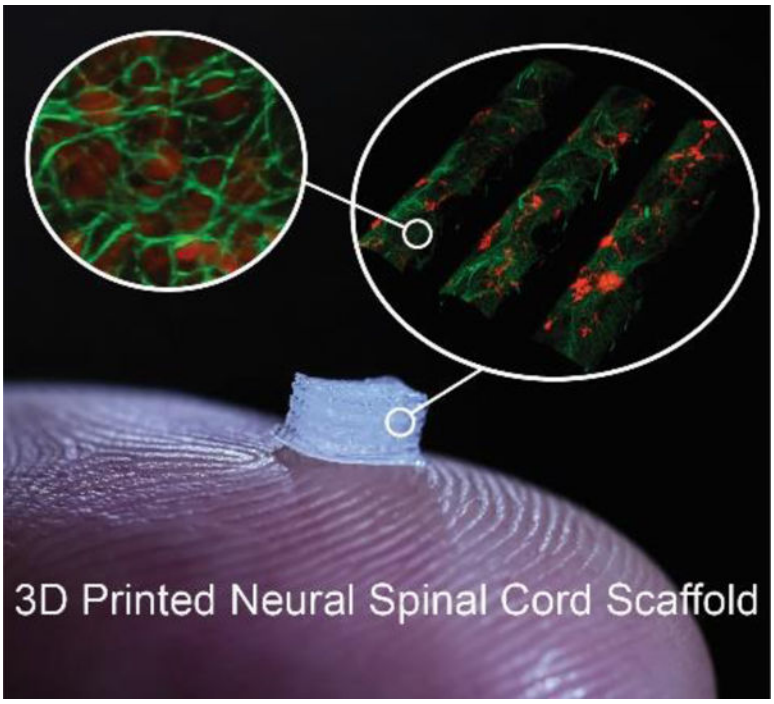

Keywords

3D bioprinting; spinal cord scaffolds; tissue engineering; induced pluripotent stem cells; neural progenitor cells

1. Introduction

In pursuing an alternative to tissue and organ transplants, tissue engineering is aimed at modeling the detailed structural features and function of native tissues.[1–3] Particularly, the ability to utilize a 3D bioprinting platform to spatially control the placement of living cells and distribution of biomaterials could allow for the construction of biologically complex microstructures beyond what is possible with conventional fabrication technologies.[4–18] In 3D bioprinting, 3D structures are fabricated in a layer-by-layer manner to allow various combinations of cells, hydrogels, and biomolecules to generate 3D tissue models. The printed structures can faithfully fabricate skin, bone, cartilage, muscle, and peripheral nerve for disease modeling, drug discovery, and regenerative transplantation.[4–13] However, strategies to tissue engineer structures of the central nervous system (CNS) are challenging due to architectural and functional complexity.[2, 3, 19] The ability to model CNS tissues *in vitro* for *in vivo* transplantation has the potential to be of critical importance in a variety of medical conditions such as spinal cord injury, traumatic brain injury, stroke, and degenerative neurologic disease. Our approach to generating functional CNS tissue constructs relies on a ‘multi-prong’ combination of sophisticated 3D bioprinting and cell culture expertise. Here, as an example for utilizing novel 3D neuro-bioprinting, we have devised a method to model the cytoarchitecture of spinal cord tissue.

Advances in creating new therapies for the CNS have shown promise through the combination of neural stem cell transplantation and biomaterial manufacturing.[20–33] For instance, injection of neural stem/progenitor cells into a subacute spinal cord contusion in rodent models has resulted in improved locomotor functional recovery.[27–29] However, one problem has been that direct injection of cells into a lesion cavity has the disadvantage of both lack of structure and a support system.[29] To bridge this gap, implantation of biocompatible scaffolds (including 3D printed scaffolds) and/or their combination with neural stem/progenitor cells and growth factors has been pursued to provide cell transplant, biological cues, and physical guides, opening opportunities to test new therapeutic options.[30–39] Yet, few of these studies have been extended to chronic injury, which is an unmet public health need.

Structurally, spinal cord tissues are not homogeneous but contain different cell types, arranged with a high order of spatial distribution.[19, 20, 32, 40] For spinal cord tissue engineering, consideration of the spatial distributions of cellular components may be critical in order to model spinal cord architecture within engineered tissue constructs (Figure 1a). Therefore, effectively recreating the *in vitro* model before *in vivo* functional outcome would be a critical advance. In contrast to other methodologies which involve printing cell-free scaffolds and then seeding them with cells after fabrication, 3D bioprinting allows us to print the cells directly onto the scaffold for optimal localization.

It has been demonstrated that efficient regeneration of specific tracts of the spinal cord is dependent on the homology of the neural cell type transplanted to the host tissue and its spatial placement during transplant. The use of induced pluripotent stem cell (iPSC)-derived spinal neuronal progenitor cells (sNPCs) can match the homology of spinal host tissue and could be autologous to avoid complications with immune suppression and prevent potential ethical concerns.[41] To this end, we have developed a protocol to generate autologous human iPSC-derived sNPCs.[42] This strategy is supported by a recent corticospinal tract regeneration study demonstrating that in neuronal transplantation studies, it is critical to caudalize the neuronal progenitor cells to improve their integration.[43] In addition to neuronal cell transplantation, oligodendrocytes myelinate demyelinated axons and provide factors that are favorable for axonal regeneration. We have previously developed a protocol to generate iPSC-derived oligodendrocyte progenitor cells (OPCs) labelled with fluorescent proteins (either enhanced green fluorescent protein (eGFP) or mCherry), allowing easy identification when co-cultured with the sNPCs.[44]

Combining these technologies, we introduce a 3D bioprinted living platform incorporating iPSC-derived sNPCs and OPCs. Our interdisciplinary approach involves the 3D manufacture of neural tissue constructs in which specific cell types (i.e., sNPCs and OPCs) can be precisely positioned within a neuro-compatible scaffold via a one-pot printing process (Figure 1b–f). This method allows us to place multiple specific neural progenitor cell types in channels at a resolution of ~200 μm. A cluster of cells, of a single type or multiple types, is deposited using a point-dispensing printing method with a 200 μm center-to-center spacing within a channel. The long-term goal is for sNPCs to differentiate into neurons projecting axons throughout the scaffold channels, and for OPCs to differentiate into oligodendrocytes to myelinate the axons, thereby creating an effective relay across the injury

site (Figure 1g). This unique bioengineered process allows us to control multiple factors including cell position and the direction of axon growth within the scaffold, providing a design construct for enhanced mimicry of tissue architecture and function to offer a relay across the injury site.

2. Results and Discussion

2.1. Assembly of 3D Printed Scaffold Construct

The 3D scaffold was printed by sequentially depositing scaffold ink and multiple cell-laden bioinks in a layer-by-layer manner to create multiple channels (see Figure 1b–f and Movie S1 – for visualization purposes, blue and red dyes replaced cells in the bioink for the movie). First, the base layer of the scaffold was created via a continuous printing method, creating a flat surface upon which channels were subsequently printed. Previous studies involving scaffolds and nerve regeneration demonstrated that ~200–300 μm diameter micro-channel scaffolds were effective in linearly guiding axons.[45, 46] On the other hand, channels larger than ~ 400 μm in diameter channel resulted in decreases of nerve regeneration.[47] Thus, the volume of a printed single channel was ~150 × 300 × 5,000 (w×h×l) μm^3. Then, a cluster of cells – of a single type or multiple types - was deposited using a point-dispensing printing method with 200 μm center-to-center spacing within a channel. The mean core volume of each dispensing of cell-laden inks was ~9.2 nl. The total volume of a single channel was ~0.23 μl. Next, another base layer and channels were printed, respectively. This process was repeated for the desired 3D scaffold architecture.

2.2. Optimizing Bioink for iPSC-Derived Neural Progenitor Cells

The first step in our bioprinting studies was to evaluate the viability of the printed neural progenitor cells in different cell-laden hydrogels (bioinks). Human iPSC-derived sNPCs, mouse iPSC-derived OPCs, or fibroblasts were suspended at a concentration of 10^7 cells/ml in different hydrogels, and a ~1 μl droplet of cell-laden hydrogel was printed onto plastic culture dishes. The viability of the printed cells was evaluated by LIVE/DEAD® cell staining 3 hours, 1 day, and 4 days after printing (Figure 2a). Gelatin methacrylate (GelMa) and gelatin mixed with fibrin (GEL/FIB) hydrogels were initially selected due to their high cell adhesion, biocompatibility, and extensive use in tissue engineering.[8, 10, 48, 49] The viability of the sNPCs in these hydrogel matrices initially ranged from 75–88% 3 hours after printing, decreasing to 50% after 1 day of culture and 20% after 4 days (Figure 2a). To analyze the morphology of the cells in the hydrogel matrices, we also conducted fluorescence microscopy imaging for up to 4 days. The printed cells did not proliferate, and axon propagation was not observed in the matrix (Figure S1, Supporting Information). We tested human fibroblasts as a reference cell type using the same printing conditions, cell densities, and hydrogel. The viability of the human fibroblasts in the matrices remained >90% on day 4 (Figure 2a), and the cells proliferated (Figure S2, Supporting Information), similar to what has been reported in 3D hydrogel matrices.[8, 10, 48, 49] This observation confirms that the printing process is not inherently incompatible with cell viability. Rather, the low viability range for a 4-day culture period seen for the iPSC-derived neural progenitors may be due to a greater sensitivity to the printing procedure, or a lack of biological components necessary for neural cell proliferation and adhesion.

To find a more effective cell-laden hydrogel for iPSC-derived neural progenitor cells, we tested Matrigel™, as it is a widely used substrate for 2D and 3D neural cell culture applications. Matrigel™ is derived from Engelbreth-Holm-Swarm (EHS) mouse sarcoma cells and is composed of growth factors and proteins which mimic the basement membrane.[50–53] It is a low viscosity liquid at 4 °C that polymerizes between 22 °C to 37 °C. Using a custom-made cooling system, we maintained the printing temperature at 4 °C and the printing pressure lower than 1 psi. As a result, there was neither significant clogging nor gelation along the nozzle during printing. An alternative to Matrigel may be necessary for a clinical product. Hydrogels made from decellularized tissues have been appropriately manufactured for clinical tissue repair and regeneration.[54] One potential future approach is to recapitulate a “natural” hydrogel manufactured from decellularized spinal cord tissue extracellular matrix (ECM) with collagen for crosslinking and optimization for 3D neural bioprinting.[55]

To improve cell viability and proliferation, sNPCs and OPCs resuspended in Matrigel were printed using four different concentrations diluted with cell culture media: 100% (undiluted), 75%, 50%, and 25% (v/v). Both sNPCs and OPCs printed in each mixture showed viability >75% 4 days post-printing (Figure 2b). However, different cell morphologies were observed for each Matrigel concentration: (i) a 25% concentration was too dilute for polymerization and did not form a 3D matrix. Rather, it acted similar to a 2D culture system; and (ii) at the higher concentrations of 75% and 100%, sNPCs tended to aggregate and axon length was shorter compared to concentrations of 25% and 50% (Figure S3, Supporting Information). Based on the appropriate balance of cell viability and morphology, 50% Matrigel concentration was chosen for the cell-laden bioink. The overall cell viability over 4 days in culture was >75% for both iPSC-derived sNPCs and OPCs when printed in 50% Matrigel (Figure 2c).

2.3. Optimizing Printing Process Time for Scaffold Construction

Prolonged scaffold printing processes may cause drying of the cell suspension in the hydrogel bioink, compromising cell viability. To identify the optimal printing process time for scaffold manufacture, consideration was made for printing cells in Matrigel with a volume of a single ~150×300×5,000 μm^3 channel. A total volume of ~0.2 μl of cells in 50% Matrigel - the amount that would be deposited within each channel - was printed onto plates and exposed to air for 5, 15, or 30 minutes before covering with cell culture media. LIVE/DEAD® staining was then conducted (Figure 2d). Cells remained viable up to 15 minutes. However, after 30 minutes of air exposure post-printing, most of the cells were dead. The cell viabilities for ~0.2 μl dispensed and exposed to air for 5, 15, and 30 minutes were 98 ± 5, 45 ± 10, and 0%, respectively. This is likely due to Matrigel dehydration (See Figure S4, Supporting Information). The printing process was therefore designed to be completed within a window of 15 minutes. When a larger volume of cells in Matrigel (~2 μl) was printed, > 95% of cells survived 30 minutes of air exposure (Figure 2e), but for the purposes of our study, increasing the volume of the cells in Matrigel was not conducted. Progenitor cells printed in Matrigel exhibited proliferation and differentiation over a period of 4 days in culture (Figure S5, Supporting Information).

2.4. Precision Placement of Bioprinted sNPCs and OPCs within Scaffold Channels

Following optimization of the hydrogel for cell suspension, sNPCs and OPCs in Matrigel were printed directly in 3D printed scaffolds with ~150 μm diameter channels to test spatial cellular distribution within the channels and the differentiation of the cells after the 3D bioprinting process. We initially utilized 3D printed scaffolds made of biocompatible silicone, which has previously been used for peripheral nerve regeneration pathways.[4, 5] The process outline and corresponding optical images are shown in Figure S6 (Supporting Information). Printed sNPCs and OPCs survived and differentiated in the channels after 4–7 days in culture post-printing. Confocal microscopy was used to determine the morphology and alignment of cells adhering on the surface of the scaffold channels.

In Figure 3, the precise spatial distribution of cell types in specific channels was demonstrated by separately dispensing sNPCs and OPCs. The left channel contained only sNPCs, the middle channel contained only OPCs, and the right channel contained both sNPCs and OPCs via separate dispensing of two different cell types within a channel of a scaffold (Figure 3a). The image was taken after 1 day of culture. sNPCs were detected using the human-specific antibody SC121 (red) and the miPSC-derived OPCs expressed eGFP (green). Printed cells were detected along the channels. In the right channel, groups of sNPCs and OPCs were interspersed with a point-dispensing distribution resolution of ~200 μm. The ability to control cell type positioning in precise locations allowed for the modeling of native tissue architecture with multiple cell types. Figures 3b,c show representative scaffolds, where sNPCs and sNPCs/OPCs were printed in different scaffolds and cultured for 4 days. Axons were detected with an antibody to βIII-tubulin (green), and the miPSC-derived OPCs expressed mCherry (red). We observed that the progenitor cells proliferated rapidly and generated axons in the 3D space over a period of 4 days.

Figure 3d i–iv shows representative close-up images of 3D bioprinted miPSC-derived OPCs after culturing for 1 day. The nuclei were detected expressing the OPC transcription factor Sox10 (red), and cell processes expressed eGFP (green). Figure 3e i–iv shows representative close-up images of 3D bioprinted sNPCs in a channel after 7 days of culture, with antibody detection of the mature neuronal marker NeuN (red), and axons detected with an antibody to βIII-tubulin (green). These observations demonstrated that 3D bioprinted sNPCs have differentiated into neurons with extended axons propagating in a designed scaffold with ~150 μm sized channels. Finally, a mixture of sNPCs and OPCs was printed onto the scaffold and cultured for 7 days (Figure 3f i–iv). The outgrowth of axons with the presence of associated OPCs was detected within the printed microchannels.

The results indicated that our 3D bioprinting methods achieved cellular viability, and the printed progenitor cells retained cell-specific phenotypic characteristics in response to the printed microenvironment. Indeed, our bioprinting approach could ultimately allow for the fabrication of a patient-specific scaffold in which specific cell types are embedded in precise positions within the designed matrix during scaffold assembly. Moreover, the approach introduced here is the first demonstration of 3D printed neuronal progenitor cells that have differentiated with axons propagating in a designed scaffold. Yet, the differentiation of OPCs into myelinating oligodendrocytes in co-culture will require further study, including longer *in vivo* timepoints.

2.5. Construction of 3D Alginate-Based Scaffolds Compatible with Bioprinting iPSC-Derived Neural Progenitor Cells

In some experiments, we have printed the progenitor cells in a biocompatible silicone scaffold matrix. In order to rapidly prototype neurocompatible scaffolds for simultaneous scaffold construction with printed progenitor cells, we also explored the use of biocompatible, soft hydrogels. We chose to test alginate (AG) prepared from a natural polymer based on its reported biocompatibility with nerve tissue.[37, 48, 56] In pure form, the stiffness and printing fidelity of alginate may not be suitable for use in an implantable scaffold, and we found the production of a scaffold containing hundred micrometer-sized channels difficult to achieve. To enable the 3D printing, we blended AG with methylcellulose (MC) and crosslinked using calcium (Ca^{2+}) or barium (Ba^{2+}) ions. MC is commonly employed as a viscosity-enhancing polymer in the food and pharmaceutical industries.[56, 57] By testing different compositions, the AG:MC ratio of 1:3 (w/v) was found to be most appropriate for printing quality. We used this ratio and adjusted the ink composition (e.g., component weight ratio and crosslinking agent) to obtain stable printing fidelity for microscale (~150 μm) channel structures. The mechanical and degradation properties of difference blends of AG/MC are shown in Figure S7–S10 (Supporting Information).

The AG/MC scaffold contained 3 × 3 continuous channels, each measuring approximately 150 μm in width, and the scaffold was designed to be ~1.5 mm × 5 mm (Figures 4a–f). sNPCs were printed into the channels during scaffold fabrication, and the structure was then immersed in culture medium and incubated for multiple days before analysis of cell placement and differentiation. After culture, analysis of scaffold sections showed that the sNPCs were alive 3 days after printing in all three layers (Figures 4b,c). Analysis of representative sections showed cells with axonal extensions present throughout the scaffold (Figure 4d). A longitudinal section of the AG/MC scaffold showed cells patterned throughout the length of the channels (Figure 4f). These observations confirmed attachment, survival, and differentiation of the sNPCs in the engineered tissue construct.

In addition, analysis of sNPCs printed in an AG/MC scaffold was conducted over 3 days (Figure 4g–i), showing progressive axon propagation in the channel. These results indicated that the optimized hydrogel-based scaffold maintained cell viability and mechanical stability during the assembly process and provided a favorable environment for axon propagation. Indeed, for the first time, our approach allowed simultaneous 3D matrix and bioprinting of human iPSC-derived neural progenitors during scaffold assembly to enable precise placement of cells. In addition to sNPCs, 3D scaffolds containing OPCs are also shown in a 3-day time progression in Figure S11 (Supporting Information). The number of OPCs with elongated processes increased during this time span and is typical of healthy OPC morphology. This supports the hypothesis that the alginate-based scaffolds are neuro-compatible for both cell types.

2.6. Calcium Imaging of 3D Bioprinted iPSC-Derived Spinal Neurons

Intracellular calcium signaling controls key cellular functions in all types of neurons.[58] We used Flou-4 calcium imaging to determine whether the neurons which differentiated from

our printed sNPCs were functional within the scaffolds 2 weeks after the 3D bioprinting process. Cells were incubated with Flou-4 dye, and calcium influxes were measured by monitoring fluorescence. Confocal microscopy of a single scaffold channel shows multiple somas and long axons measured at baseline levels (Figure 5a) spontaneously increasing in fluorescent intensity, marking intracellular calcium influxes (Figure 5b). (Movie S2 shows calcium influxes in axon projections).

Cells were then exposed to various signaling molecules to further characterize the specificity of the cell types. Cells responded to high potassium (Figure 5c,d) with a 7-fold increase in fluorescent intensity and responded to the neurotransmitter glutamate (Figure 5e,f). Time-dependent measurements of ten cells in this area show all the cells responding to both high potassium and glutamate (Figure 5g). The evidence of active neurons in the scaffold shows that the 3D bioprinted neuronal progenitors can survive and differentiate into functionally mature neurons.

3. Conclusions

A 3D spinal cord tissue-like platform was created via a one-pot 3D bioprinting approach involving neuronal and glial progenitor cells in a biocompatible scaffold. This approach allowed us to create fully 3D bioprinted neural progenitor cells with axon propagation in a designed 3D biocompatible scaffold. We believe these “living” platforms will serve as *in vitro* models for complex central nervous system (CNS) architecture including spinal cord injury (SCI) and have the potential to be employed as clinical implants to treat patients. In the spinal cord, it has been demonstrated that cell-to-cell contact is crucial for outgrowth of axons from grafted cells and ingrowth of axons into the transplant.[43, 59] Since each injury cavity is individual, it would therefore follow that each patient would benefit from a patient-specific design. The accurate reproduction will provide stable contact between the implanted cell-printed scaffold and the native spinal cord. Thus, future studies will focus on: (1) tailoring the shape of the scaffold for each patient injury via co-development of 3D scanning technologies such as a magnetic resonance imaging (MRI); (2) transplanting the scaffold in an *in vivo* model of contusion SCI to assess the survival and fate of the cells, as well as the effect on functional recovery; and (3) incorporating 3D printed stimuli-responsive capsules containing biological and biochemical cues for programmable release of multiplexed gradients within the designed 3D architecture to promote neuronal differentiation and axon guidance for CNS therapies.[4, 60, 61] Overall, we anticipate that our platform can be used to prepare novel biomimetic scaffolds modeling complex CNS tissue architecture *in vitro*, with the long-term goal of creating a clinical implant to treat patients with CNS injuries such as chronic SCI.

4. Experimental Section

Cell preparation:

Three cell types were used in this study: primary human neonatal dermal fibroblasts (ATCC; PCS-201–010; Manassas, VA, USA), hiPSC-derived ventral sNPCs [42] and miPSC-derived OPCs [44].

Fibroblasts were seeded at a density of 5,000 cells per cm^2 on tissue culture treated plates and cultured in FibroGRO™ Xeno-Free Human Fibroblast Expansion Medium (Millipore Sigma SCM037; MA, USA). Cell culture media was changed every other day, and fibroblasts were passaged at 80% to 100% confluence using TrypLE Select (1×) (ThermoFisher Scientific; A1285901; MA, USA). On the day of printing, fibroblasts were dissociated with TrypLE, washed, and re-suspended at a concentration of 10^7 cells/ml in the desired bioink. Cells were kept on ice prior to the 3D bioprinting process.

The derivation of sNPCs has been previously described.[42] Briefly, hiPSC line UMN-X7 was maintained on cell culture treated flasks (Corning; 430639; MA, USA) coated with recombinant human vitronectin (rhVTN) (Peptrotech; AF-140–09; NJ, USA) in Essential 8 Medium (ThermoFisher; A2858501). For differentiation, hiPSCs were passaged onto rhVTN at half the colony density used for maintenance. Media was changed 18 to 24 hours later each day in the following manner: Days 1–3, differentiation medium consisting of Essential 6 (ThermoFisher Scientific; A1516401) supplemented with 250 nM LDN-193189 (Selleckchem; S7507; TX, USA). Days 4–11, following a passage, differentiation medium consisted of Essential 6 supplemented with 250 nM LDN-193189, 100 nM retinoic acid (RA) (Sigma-Aldrich; R2625), and 3 mM CHIR99021 (Tocris; 4423; Bristol, UK). Days 11–16, media consisted of N2B27 neural media made of Dulbecco's modified Eagle's medium (DMEM) F/12 (ThermoFisher Scientific; 11039–047) basal containing (1×) N2 Supplement (ThermoFisher; A13707–01), (1×) B27 Supplement (ThermoFisher; 17504044), 100 nM retinoic acid and 1 μM smoothened agonist (SAG, Cayman Chemical; 11914; MI, USA). Cells were cryo-banked on day 17. One day prior to printing, sNPCs were thawed and suspended in N2B27 medium supplemented with 1 μM RA and 1μM SAG on a low attachment plate. On the day of printing, sNPCs were dissociated with TrypLE, washed, and re-suspended at a concentration of 10^7 cells/ml. Cells were kept on ice prior to the 3D bioprinting process. After printing, sNPCs were fed with N2B27 supplemented with 20 ng/mL glial cell-derived neurotrophic factor (GDNF) (Peprotech; 450–10), 20 ng/mL brain-derived neurotrophic factor (BDNF) (Peprotech; 450–02), and 20 ng/mL NT3 (Peprotech; 450–03).

The derivation of OPCs has been previously described.[44] Briefly, miPSC line UMN-3F10 was cultured on irradiated murine embryonic fibroblasts in miPSC medium consisting of DMEM with high glucose and sodium pyruvate (ThermoFisher Scientific; 10828028), 10% fetal bovine serum (HyClone; SH30071.03; UT, USA), (1×) MEM nonessential amino acids (NEAA) (ThermoFisher Scientific; 11140050), (1×) GlutaMAX (ThermoFisher Scientific; 35050061), 0.1 mM 2-mercaptoethanol (βME) (Life Technologies; NY, USA), (1×) penicillin/streptomycin (P/S) (Corning; 30–002-CI), and 1,000 U/ml ESGRO-leukemia inhibitory factor (LIF) (Millipore; ESG1107). UMN-3F10 is from a mTmG transgenic mouse, and certain batches of cells were constitutively labeled with transmembrane eGFP by supplementing their miPSC medium with 10 nM tamoxifen (Sigma-Aldrich; T5648). For differentiation, hiPSCs were dissociated and aggregated onto ultra-low attachment plates (Corning; 07–200-601). Media was changed 18 to 24 hours later each day in the following manner: days 1–3, knockout serum replacement (KSR) differentiation medium consisting of Minimum Essential Medium (MEM) (Corning; 10–010-CV), 20% KnockOut Serum Replacement (ThermoFisher Scientific; 10828028), 1 mM sodium pyruvate (ThermoFisher

Scientific; 11360070), (1×) MEM NEAA, 0.1 mM βME, and (1×) P/S. Day 4, KSR medium with 0.2 μM retinoic acid. Day 5, KSR medium with 0.2 μM retinoic acid and 1 μM purmorphamie (Cayman Chemical; 483367–10-8). Days 6–7, N2 medium consisting of MEM, (1×) N2 Supplement, 1 mM sodium pyruvate, (1×) MEM NEAA, 0.1 mM βME, 1× P/S with 0.2 μM retinoic acid and 1 μM purmorphamine. On day 8, aggregates were plated onto poly-L-ornithine (Sigma-Aldrich; P4957)/fibronectin (Sigma-Aldrich; F1141) coated plates into OPC expansion media consisting of N2B27 medium with 20 ng/ml fibroblast growth factor-2 (FGF-2) (R&D Systems; 233-FB; MN, USA), 20 ng/ml rhPDGF-AA (Sigma-Aldrich; GF142), 100 ng/ml rhShh (R&DSystems; 1845-SH), and (1×) penicillin/streptomycin. After plating, medium was changed every other day. The OPCs were grown to confluence and banked. One day prior to printing, OPCs were thawed and suspended in OPC expansion media. On the day of printing, OPCs were dissociated with Accutase® (Stemcell Technologies; 07920), washed, and re-suspended at a concentration of 10^7 cells/ml. Cells were kept on ice prior to the 3D bioprinting process. After printing, OPCs were fed with OPC expansion media.

Bioinks preparation for cell-laden matrix:

Three hydrogels were used in this study for cell-laden bioinks: Matrigel matrix (Corning; 354234), gelatin/fibrin (GEL/FIB), and GelMa bioinks.

The GEL/FIB bioink was based off a previously published protocol.[10] Stock solutions of 15% (w/v) gelatin (2×), 50 mg/mL fibrinogen (5×), and 250 mM $CaCl_2$ (100×) were prepared in the following manner: Gelatin (Sigma-Aldrich; G2500; MO, USA) was dissolved in Dulbecco's Phosphate Buffered Saline (DPBS) without calcium and magnesium (ThermoFisher Scientific; 14190144) for 12 hours at 70 °C. The pH was adjusted to 7.5 using 1M NaOH. The solution was sterile filtered and stored at 4 °C until use. Fibrinogen (Sigma-Aldrich; F8630) was dissolved in DPBS without calcium and magnesium for 4 hours at 37 °C. The solution was sterile filtered and stored at −20 °C until use. $CaCl_2$ (Sigma-Aldrich; 449709) was dissolved in cell culture grade water. The solution was sterile filtered and stored at 25 °C until use. Then, the bioink was prepared by dissolving hyaluronic acid (HA) in N2B27 at 37 °C prior to the addition of the gelatin, fibrinogen, and $CaCl_2$ stock solutions. The final concentrations for each component were 7.5% (w/v) gelatin, 10 mg/mL fibrinogen, 2.5 mM $CaCl_2$, and 3 mg/mL HA in N2B27. The solution was stored at 37 °C until fully dissolved. After printing, the hydrogel was polymerized with a thrombin/transglutaminase (TG) solution for 15–20 minutes. Solutions of thrombin and TG were prepared prior to the printing process. To create the thrombin stock solution, lyophilized thrombin (Sigma-Aldrich; T4648) was reconstituted at 100 U/ml using DPBS and stored at −20 °C. The 60 mg/ml TG solution was created by dissolving lyophilized Moo Glue powder (Modernist Pantry; ME, USA; 1201–50) in DPBS, and stirring at 37 °C until completely dissolved. Then, the solution was sterile filtered and stored at −20 °C. Prior to use, the TG solution was added to the thrombin solution in order to achieve a final concentration of 0.2% (w/v).

GelMa consisted of 7.5% (w/v) GelMa (Allevi) with 0.05% lithium phenyl-2,4,6-trimethylbenzoylphosphinate (LAP; Allevi) in DPBS. The solution was briefly vortexed and

stored at 37 °C until fully dissolved. During the printing, the hydrogel was crosslinked via UV irradiation.

Ink preparation for scaffolds:

Three materials were tested for the scaffold: acetoxy-based room temperature vulcanizing (RTV) silicone (Loctite; LOCTITE SI 595 CL; OH, USA), poly(ethylene glycol) diacrylate (PEGDA), and alginate admixed with methylcellulose (AG/MC).

The PEGDA hydrogel mixture consisted of 20% (w/v) PEGDA (MW 700; Sigma-Aldrich; 455008), 5.5% (w/v) polyethylene oxide (Mv 1,000,000; Sigma-Aldrich; 372781), 10% (w/v) glycerol (Sigma-Aldrich), and photoinitiators in DPBS. Three different types of photoinitiators were used for comparison: 0.05% (w/v) LAP, 0.3% (w/v) 2-hydroxy-1-[4-(2-hydroxyethoxy) phenyl]-2-methyl-1-propanone (Irgacure 2959; BASF; NJ, USA), and 2.5% (w/v) 2,2-Azobis[2-methyl-N-(2-hydroxyethyl) propionamide] (VA-086; Wako Chemicals; VA, USA).

For the AG/MC scaffolds, three different types of AG/MC (named AG1, AG2, and AG3), and a volume ratio of 1:3 (AG:MC) was used. The AG1 mixture consisted of 6% (w/v) of low viscosity alginate (alginic acid sodium salt from brown algae, 4–12 cP; Sigma-Aldrich; A1112) and 18% (w/v) of medium viscosity MC (4000 cP; Sigma; M0512) in DPBS. For cross-linking of alginate, $CaCl_2$ was dissolved in DPBS (20 mg/mL). The AG2 mixture consisted of 6% (w/v) of medium viscosity alginate (2,000 cP; Sigma-Aldrich; A2033) and 18% (w/v) of medium viscosity MC in DPBS. $CaCl_2$ was used for the cross-linking agent (20 mg/mL). The AG3 mixture consisted of the same components as AG2. However, $BaCl_2$ (Sigma-Aldrich; 202738) was used for the cross-linking agent (10 mg/mL). All inks were mixed using a planetary centrifugal mixer (ARE-310l; Thinky) and centrifuged to remove any air bubbles before printing at room temperature. After printing of all blends completed, the sample was placed (soaked) in a cross-linking agent for 10 minutes at 4 °C. Following cross-linking, the samples were rinsed with DPBS at least 10 times.

3D printing procedure:

A custom microextrusion-based 3D printing system was used as described previously.[4, 5, 60] Briefly, the system consisted of a three-axis dispensing robot (F5200N; Fisnar; NJ, USA), pneumatic dispensing system (Ultimus V; Nordson EFD; OH, USA), vision system, and personal computer (Figure S12). The dispensing apparatuses were connected to the printers to extrude the different bio-inks through the micronozzle with a 100 μm inner diameter (5132–0.25-B; Nordson EFD). Printing speeds for the scaffold inks ranged from 1–3 mm/s (line-dispensing printing mode). The dispensing time for cell-laden hydrogel inks ranged from 0.1–0.3 seconds (point-dispensing printing mode). The printing pressures for cell-laden hydrogel and scaffolds were 0.5–1 psi and 80–200 psi, respectively. All print paths were controlled using G-code commands, which were generated by the software Slic3R from 3D models. The system also contained a customized heating and cooling system to maintain a printing temperature of ~37 °C (for GelMa and GEL/FIB) and 4 °C (for Matrigel), respectively. The system allowed for the ability to print the cell-laden hydrogel below 1 psi. For the photo-crosslinkable hydrogel (i.e., GelMa and PEGDA)

printing, the hydrogel was crosslinked via a UV irradiation period (UVL-56; UVP). For the silicone scaffolds, following completion of the silicone printing process, the printed structure was cured under ambient condition for 5 hours.

Immunocytochemistry:

Cultures were fixed in 10% buffered Formalin (Protocol 23–305-510) for 10 minutes, permeabilized in PBS + 0.2% (v/v) Triton X-100, blocked in PBS + 1% BSA, 0.1% Tween-20 for 30 minutes, and incubated with primary antibodies for 2 hours. Cultures were washed twice with blocking solution and incubated 1 hour with secondary antibodies. 4',6-diamidino-2-phenylindole (DAPI) was added for five minutes before final washing in PBS-T. Antibodies: STEM121 (Takara; Y40410; 1:500), βIII Tubulin (Millipore; MAB1637; 1:500), NeuN (Abcam; ab177487; 1:1000), Sox10 (R&D Systems; AF2864-SP; 1:100). Appropriate secondary antibodies were purchased from ThermoFisher Scientific and used at 1:500 dilution.

Microscopy:

Direct fluorescence imaging of samples was performed using either a DMI 6000B inverted microscope with a DFC 365 FX camera and Leica Application Suite software (Leica; Wetzlar, Germany) or a Nikon C2 Upright Confocal Microscope with NIS-Elements AR imaging software.

Viability assay:

The LIVE/DEAD® Viability/Cytotoxicity Kit (ThermoFisher Scientific; L3224) was used to test viability after 3D bioprinting. In brief, cells were washed once and incubated with 2 μM calcein AM and 4 μM EthD-1 diluted in DMEM/F12 for 20 minutes. Cells were washed and representative images were taken of samples. The number of live (green) and dead (red) cells were counted in each field using Cell Counter in Image-J.

Calcium Imaging:

Protocols were based off the Flou-4 calcium imaging kit instructions (ThermoFisher Scientific; F10489). In brief, 3D printed scaffold constructs on glass coverslips were incubated in fresh Flou-4, AM Loading Solution in BrainPhys Neuronal Medium with N2 supplement-A and SM1 Neuronal supplement (Stemcell Technologies; 05793) for 20 minutes. Cells were washed with complete BrainPhys Neuronal Medium and imaged using two methods: to test calcium responses to specific stimuli, individual constructs on coverslips were transferred to a submersion-type recording chamber maintained at room temperature and continuously superfused (2.0 ± 0.25 ml/min) with oxygenated (100% O_2, pH 7.4) physiological saline. The physiological solution contained in mM: 115.0 NaCl, 2.0 KCl, 1.5 $MgCl_2$, 3.0 $CaCl_2$, 10.0 4-(2-hydroxyethyl)-1-piperazineethanesulfonic acid (HEPES) and 10.0 glucose (pH 7.3, 300–310 mOsm). Physiological saline containing 70 mM KCl and 100 μM glutamate (Sigma Aldrich; G1626) (pH 7.3, 300–310 mOsm) were perfused through the system. Scaffolds were imaged using a two-photon laser scanning microscopy system (Prairie Ultima; Prairie Technologies) coupled with a Ti:sapphire laser (MaiTai HP; Spectra Physics).

A Nikon C2 Upright Confocal Microscope with NIS-Elements AR imaging software was used to view spontaneous calcium fluxes at high resolution. Five-minute movies were recorded, and neuronal calcium events were defined as sharp transient increases in fluorescence intensity in a soma.

Mechanical proprieties:

A dynamic mechanical analyzer (RSA-G2; TA Instruments) was used to test the compression of a rat spinal cord and 3D printed empty scaffolds made of PEGDA and AG/MC blends. The compression test was performed with the longitudinal direction. Prior to all tests, the load was reset and the load cell was calibrated. Multiple samples of each material were characterized (n=10) and stress-strain characteristics were measured. The Young's modulus was taken as the slope of the linear region of the stress-strain curve.

Statistics:

All data are expressed as mean ± standard deviation. Statistical analyses were performed using R Statistical Software. Normal data distribution was determined using an analysis of variance (ANOVA) test. A Tukey Honest Significant Difference (HSD) test was used to compare the mean values of all study parameters to spinal cord values. P value < 0.05 was considered statistically significant from the spinal cord.

Supplementary Material

Refer to Web version on PubMed Central for supplementary material.

Acknowledgements

A.M.P. and M.C.M. are co-senior authors. The authors thank David Yang, Elizabeth Smith, Samantha Barkan, and Dr. Susan A. Keirstead for insightful discussions and technical support regarding the 3D bioprinting process, statistical analysis, and the calcium imaging studies. J.R.D., A.M.P., and M.C.M. acknowledge Conquer Paralysis Now, and the Minnesota Spinal Cord Injury and Traumatic Brain Injury Research Grant Program. J.R.D. and A.M.P. acknowledge generous support from an anonymous philanthropic donor. M.C.M. acknowledges the National Institute of Biomedical Imaging and Bioengineering of the National Institutes of Health (Award No. 1DP2EB020537). A.M.P. acknowledges the CTSI KL2 Scholar Program of the National Institutes of Health (Award No. NIH CON000000033119–3002). The content is solely the responsibility of the authors and does not necessarily represent the official views of the National Institutes of Health.

References

[1]. Langer R, Vacanti JP, Science 1993, 260, 920. [PubMed: 8493529]

[2]. Hopkins AM, DeSimone E, Chwalek K, Kaplan DL, Prog. Neurobiol. 2015, 125, 1. [PubMed: 25461688]

[3]. Giger RJ, Hollis ER, Tuszynski MH, Cold Spring Harb. Perspect. Biol. 2010, 2, a001867.

[4]. Johnson BN, Lancaster KZ, Zhen G, He J, Gupta MK, Kong YL, Engel EA, Krick KD, Ju A, Meng F, Enquist LW, Jia X, McAlpine MC, Adv. Funct. Mater. 2015, 25, 6205. [PubMed: 26924958]

[5]. Johnson BN, Lancaster KZ, Hogue IB, Meng F, Kong YL, Enquist LW, McAlpine MC, Lab Chip 2016, 16, 1393. [PubMed: 26669842]

[6]. Mironov V, Boland T, Trusk T, Forgacs G, Markwald RR, Trends Biotechnol. 2003, 21, 157. [PubMed: 12679063]

[7]. Derby B, Science 2012, 338, 921. [PubMed: 23161993]

[8]. Kolesky DB, Truby RL, Gladman A, Busbee TA, Homan KA, Lewis JA, Adv. Mater. 2014, 26, 3124. [PubMed: 24550124]

[9]. Kang HW, Lee SJ, Ko IK, Kengla C, Yoo JJ, Atala A, Nat. Biotechnol. 2016, 34, 312. [PubMed: 26878319]

[10]. Kolesky DB, Homan KA, Skylar-Scott MA, Lewis JA, Proc. Natl. Acad. Sci. 2016, 113, 3179. [PubMed: 26951646]

[11]. Murphy SV, Atala A, Nat. Biotechnol. 2014, 32, 773. [PubMed: 25093879]

[12]. Knowlton S, Anand S, Shah T, Tasoglu S, Trends Neurosci. 2018, 41, 31. [PubMed: 29223312]

[13]. Colosi C, Shin SR, Manoharan V, Massa S, Costantini M, Barbetta A, Dokmeci MR, Dentini M, Khademhosseini A, Adv. Mater. 2016, 28, 677. [PubMed: 26606883]

[14]. Leijten J, Seo J, Yue K, Trujillo-de Santiago G, Tamayol A, Ruiz-Esparza GU, Shin SR, Sharifi R, Noshadi I, Álvarez MM, Zhang YS, Khademhosseini A, Mater. Sci. Eng. R Rep. 2017, 119, 1. [PubMed: 29200661]

[15]. Pedde RD, Mirani B, Navaei A, Styan T, Wong S, Mehrali M, Thakur A, Mohtaram NK, Bayati A, Dolatshahi-Pirouz A, Nikkhah M, Willerth SM, Akbari M, Adv. Mater. 2017, 29, 1606061.

[16]. Zhu W, George JK, Sorger VJ, Zhang LG, Biofabrication 2017, 9, 025002.

[17]. Hsieh FY, Lin HH, Hsu SH, Biomaterials 2015, 71, 48. [PubMed: 26318816]

[18]. Lee S, Nowicki M, Harris B, Zhang LG, Tissue Eng., Part A 2017, 23, 491. [PubMed: 27998214]

[19]. Fry EJ, Clin. Exp. Pharmacol. Physiol. 2001, 28, 253. [PubMed: 11251636]

[20]. Assinck P, Duncan GJ, Hilton BJ, Plemel JR, Tetzlaff W, Nat. Neurosci. 2017, 20, 637. [PubMed: 28440805]

[21]. Karimi-Abdolrezaee S, Eftekharpour E, Wang J, Morshead CM, Fehlings MG, J. Neurosci. 2006, 26, 3377. [PubMed: 16571744]

[22]. McDonald JW, Liu X-Z, Qu Y, Liu S, Mickey SK, Turetsky D, Gottlieb DI, Choi DW, Nat. Med. 1999, 5, 1410. [PubMed: 10581084]

[23]. Ogawa Y, Sawamoto K, Miyata T, Miyao S, Watanabe M, Nakamura M, Bregman B, Koike M, Uchiyama Y, Toyama Y, Okano H, J. Neurosci. Res. 2002, 69, 925. [PubMed: 12205685]

[24]. Teng YD, Lavik EB, Qu X, Park KI, Ourednik J, Zurakowski D, Langer R, Snyder EY, Proc. Natl. Acad. Sci. 2002, 99, 3024. [PubMed: 11867737]

[25]. Rossi SL, Nistor G, Wyatt T, Yin HZ, Poole AJ, Weiss JH, Gardener MJ, Dijkstra S, Fischer DF, Keirstead HS, PLoS One 2010, 5, e11852.

[26]. Tian L, Prabhakaran MP, Ramakrishna S, Regen. Biomater. 2015, 2, 31. [PubMed: 26813399]

[27]. Mothe AJ, Tator CH, Int. J. Dev. Neurosci. 2013, 31, 701. [PubMed: 23928260]

[28]. Lu P, Wang Y, Graham L, McHale K, Gao M, Wu D, Brock J, Blesch A, Rosenzweig ES, Havton LA, Zheng B, Conner JM, Marsala M, Tuszynski MH, Cell 2012, 150, 1264. [PubMed: 22980985]

[29]. Parr AM, Kulbatski I, Zahir T, Wang X, Yue C, Keating A, Tator CH, Neuroscience 2008, 155, 760. [PubMed: 18588947]

[30]. Winter CC, Katiyar KS, Hernandez NS, Song YJ, Struzyna LA, Harris JP, Cullen DK, Acta Biomater. 2016, 38, 44. [PubMed: 27090594]

[31]. Li X, Liu S, Zhao Y, Li J, Ding W, Han S, Chen B, Xiao Z, Dai J, Adv. Funct. Mater. 2016, 26, 5835.

[32]. Führmann T, Anandakumaran PN, Shoichet MS, Adv. Healthcare Mater. 2017, 6, 1601130.

[33]. Gao M, Lu P, Bednark B, Lynam D, Conner JM, Sakamoto J, Tuszynski MH, Biomaterials 2013, 34, 1529. [PubMed: 23182350]

[34]. Moore MJ, Friedman JA, Lewellyn EB, Mantila SM, Krych AJ, Ameenuddin S, Knight AM, Lu L, Currier BL, Spinner RJ, Marsh RW, Windebank AJ, Yaszemski MJ, Biomaterials 2006, 27, 419. [PubMed: 16137759]

[35]. De Ruiter GC, Onyeneho IA, Liang ET, Moore MJ, Knight AM, Malessy MJ, Spinner RJ, Lu L, Currier BL, Yaszemski MJ, Windebank AJ, J. Biomed. Mater. Res. A 2008, 84, 643. [PubMed: 17635012]

[36]. Thomas M, Willerth SM, Front. Bioeng. Biotechnol. 2017, 5, 69. [PubMed: 29204424]

[37]. Günther MI, Weidner N, Müller R, Blesch A, Acta Biomater. 2015, 27, 140. [PubMed: 26348141]

[38]. Gelain F, Panseri S, Antonini S, Cunha C, Donega M, Lowery J, Taraballi F, Cerri G, Montagna M, Baldissera F, Vescovi A, ACS Nano 2011, 5, 227. [PubMed: 21189038]

[39]. Pawar K, Cummings BJ, Thomas A, Shea LD, Levine A, Pfaff S, Anderson AJ, Biomaterials 2015, 65, 1. [PubMed: 26134079]

[40]. Bradbury EJ, McMahon SB, Nat. Rev. Neurosci. 2006, 7, 644. [PubMed: 16858392]

[41]. Ahuja CS, Fehlings M, Stem Cells Transl. Med. 2016, 5, 914. [PubMed: 27130222]

[42]. Walsh P, Truong V, Hill C, Stoflet ND, Baden J, Low WC, Keirstead SA, Dutton JR, Parr AM, Cell Transplant. 2017, 26, 1890. [PubMed: 29390875]

[43]. Kadoya K, Lu P, Nguyen K, Lee-Kubli C, Kumamaru H, Yao L, Knackert J, Poplawski G, Dulin JN, Strobl H, Takashima Y, Biane J, Conner J, Zhang SC, Tuszynski MH, Nat. Med. 2016, 22, 479. [PubMed: 27019328]

[44]. Terzic D, Maxon JR, Krevitt L, DiBartolomeo C, Goyal T, Low WC, Dutton JR, Parr AM, Cell Transplant. 2016, 25, 411. [PubMed: 25955415]

[45]. Gros T, Sakamoto JS, Blesch A, Havton LA, Tuszynski MH, Biomaterials 2010, 31, 6719. [PubMed: 20619785]

[46]. Pawelec KM, Koffler J, Shahriari D, Galvan A, Tuszynski MH, Sakamoto J, Biomed. Mater. 2018, 13, 044104.

[47]. Krych AJ, Rooney GE, Chen B, Schermerhorn TC, Ameenuddin S, Gross L, Moore MJ, Currier BL, Spinner RJ, Friedman JA, Yaszemski MJ, Windebank AJ, Acta biomater. 2009, 5, 2551. [PubMed: 19409869]

[48]. Atala A, Yoo JJ, Essentials of 3D Biofabrication and Translation, Elsevier, Amsterdam, Netherlands 2015.

[49]. Nichol JW, Koshy ST, Bae H, Hwang CM, Yamanlar S, Khademhosseini A, Biomaterials 2010, 31, 5536. [PubMed: 20417964]

[50]. Lei Y, Schaffer DV, Proc. Natl. Acad. Sci. 2013, 110, E5039.

[51]. Choi SH, Kim YH, Hebisch M, Sliwinski C, Lee S, D'Avanzo C, Chen H, Hooli B, Asselin C, Muffat J, Klee JB, Zhang C, Wainger BJ, Peitz M, Kovacs DM, Woolf CJ, Wagner SL, Tanzi RE, Kim DY, Nature 2014, 515, 274. [PubMed: 25307057]

[52]. Uemura M, Refaat MM, Shinoyama M, Hayashi H, Hashimoto N, Takahashi J, J. Neurosci. Res. 2010, 88, 542. [PubMed: 19774667]

[53]. Ma W, Tavakoli T, Derby E, Serebryakova Y, Rao MS, Mattson MP, BMC Dev. Biol. 2008, 8, 90. [PubMed: 18808690]

[54]. Agmon G, Christman KL, Curr. Opin. Solid State Mater. Sci. 2016, 20, 193. [PubMed: 27524932]

[55]. Volpato FZ, Führmann T, Migliaresi C, Hutmacher DW, Dalton PD, Biomaterials 2013, 34, 4945. [PubMed: 23597407]

[56]. Schütz K, Placht AM, Paul B, Brüggemeier S, Gelinsky M, Lode A, Tissue Eng J. Regen. Med. 2017, 11, 1574.

[57]. Li H, Tan YJ, Leong KF, Li L, ACS Appl. Mater. Interfaces 2017, 9, 20086.

[58]. Grienberger C, Konnerth A, Neuron 2012, 73, 862. [PubMed: 22405199]

[59]. Dulin JN, Adler AF, Kumamaru H, Poplawski GH, Lee-Kubli C, Strobl H, Gibbs D, Kadoya K, Fawcett JW, Lu P, Tuszynski MH, Nat. Commun. 2018, 9, 84. [PubMed: 29311559]

[60]. Gupta MK, Meng F, Johnson BN, Kong YL, Tian L, Yeh Y-W, Masters N, Singamaneni S, McAlpine MC, Nano Lett. 2015, 15, 5321. [PubMed: 26042472]

[61]. Qiu K, Zhao Z, Haghiashtiani G, Guo SZ, He M, Su R, Zhu Z, Bhuiyan DB, Murugan P, Meng F, Park SH, Chu CC, Ogle BM, Saltzman DA, Konety BR, Sweet RM, McAlpine MC, Adv. Mater. Technol. 2018, 3, 1700235.

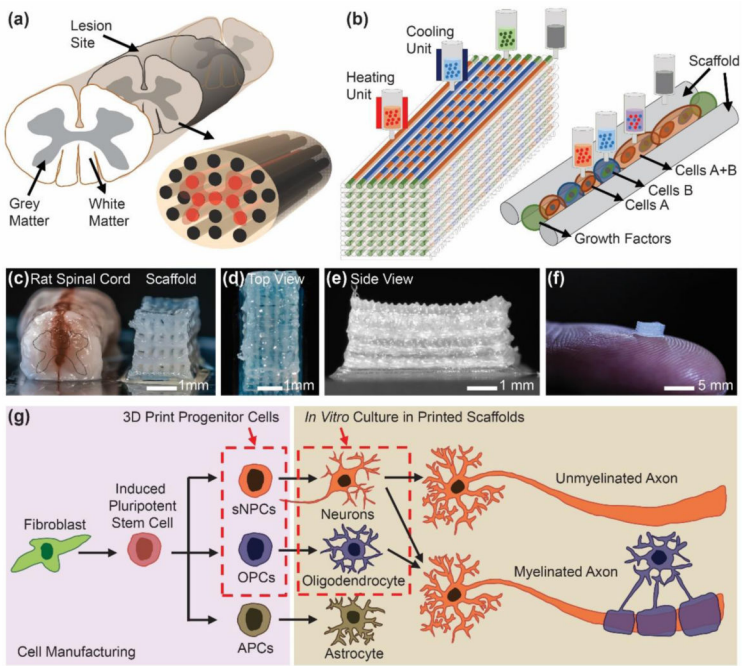

Figure 1.

Experimental strategies for 3D bioprinting spinal cord tissue. (a) Schematic of the spinal cord illustrating grey matter and white matter boundaries and a design for a 3D bioprinted multichannel scaffold for modeling the spinal cord. (b) Schematic overview of the 3D bioprinting process. Biocompatible bioinks are extruded at specific temperatures (37 °C or 4 °C, depending on the bioink) in a layer-by-layer process. The scaffold ink is structurally supportive and can be made with a biocompatible material. (c) Comparison of a transected rat spinal cord and the design principle for scaffolds consisting of multiple, continuous channels. The number of channels can be scaled according to the size of the scaffold needed. (d) Top view image of scaffold channels demonstrates a printing resolution of ~150 μm. Channels are continuous throughout the scaffold, allowing for axonal extension. (e) Side view of a 5 mm long scaffold. (f) A 2×2×5 mm^3 sized scaffold on top of a finger shows the scale of a scaffold. (g) Schematic of induced pluripotent stem cell (iPSC) reprogramming and differentiation into spinal neuronal progenitor cells (sNPCs) or oligodendrocyte progenitor cells (OPCs). These progenitor cells are 3D bioprinted into the scaffold and cultured *in vitro*.

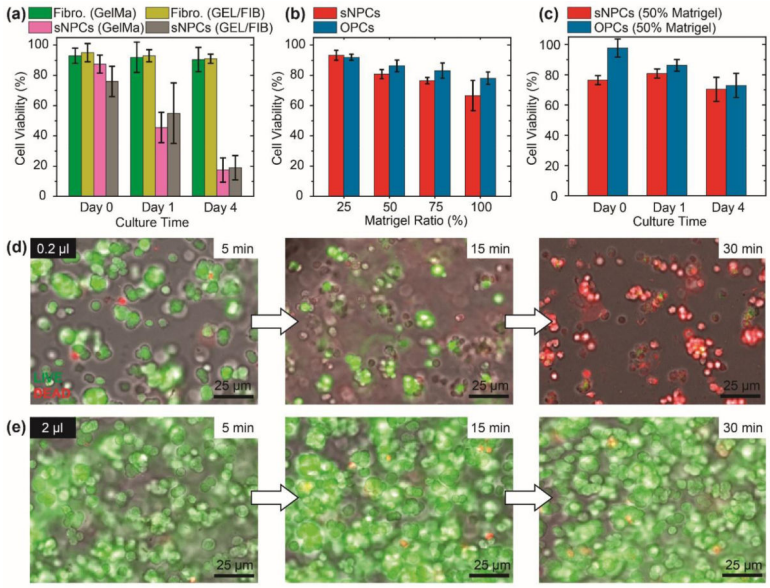

Figure 2.

Optimizing the cell-laden bioink formulation and printing process time for scaffold construction. (a) Cell viability of 3D bioprinted fibroblast-, sNPC-, and OPC-laden GelMa and GEL/FIB bioinks cultured for 3 hours (Day 0), 24 hours (Day 1), and 72 hours (Day 4). (b) Cell viability of 3D bioprinted sNPC-, and OPC-laden Matrigel suspensions with the use of 25%, 50%, 75%, and 100% Matrigel concentrations. Matrigel was diluted with N2/B27 basal media, and cell viability was measured after 1 day in culture (24 hours after printing). (c) Cell viability of cultured, bioprinted sNPCs and OPCs in 50% Matrigel suspension cultured at Day 0, Day 1, and Day 4. (d, e) LIVE/DEAD® sNPC staining after short-term post-printing of (d) ~0.2 µl and (e) ~2 µl volumes, used to determine the maximum printing times before cells needed to be placed under *in vitro* culture conditions.

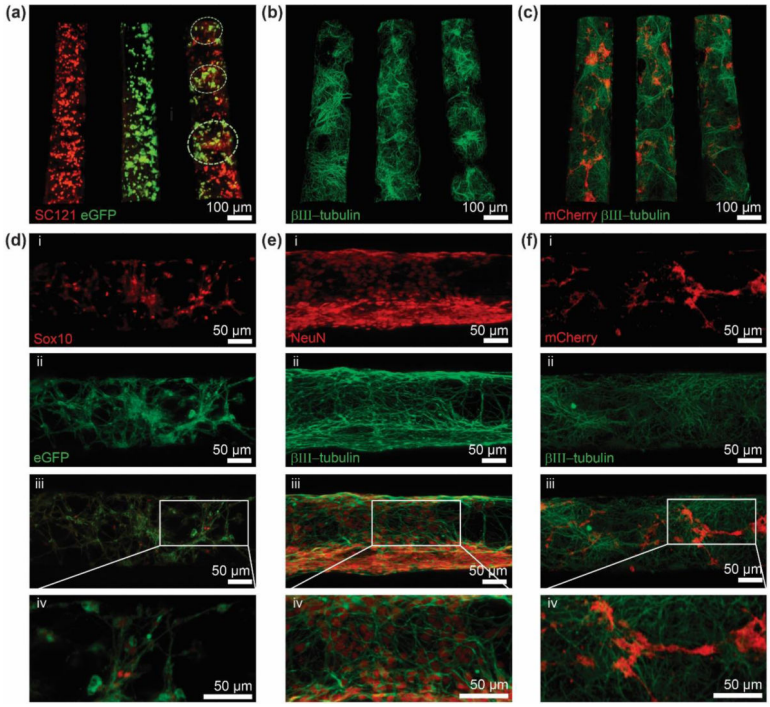

Figure 3.

3D bioprinted iPSC-derived neuronal and glial progenitor cells after *in vitro* culture. (a) Distribution of cell types in specific channels: sNPCs only (left), OPCs only (middle), and sNPCs and OPCs (right). Groups of sNPCs and OPCs are interspersed with a distribution resolution of ~200 μm in a single channel (highlighted on the right channel). sNPCs are detected with human-specific antibody SC121 (red), and OPCs express eGFP (green). The image was taken 24 hours post-printing. (b) sNPCs printed in a scaffold after 4 days of culture. Antibody to β3III-tubulin detects axonal projections in the channels. (c) sNPCs and OPCs co-printed in a scaffold after 4 days of culture. β3III-tubulin shows axonal projections down the channels, and the OPCs express mCherry. (d) Image of 3D printed OPCs in a channel after 1 day of culture. (i-iv) OPCs constitutively express the OPC marker Sox10 (red) and eGFP (green), and the merged image is shown along with a close-up. e) Image of 3D printed sNPCs in a channel after 7 days of culture. (i-iv) sNPCs differentiate into neurons and express the mature neuron marker NeuN (red), the neuron-specific microtubule element β3III-tubulin (green), and the merged image is shown along with a close-up. f) Image of 3D printed sNPCs and OPCs in a channel after 7 days of culture shows axon projections in close proximity to the OPCs. (i-iv) OPCs express mCherry (red), sNPCs differentiate into neurons and express the β3III-tubulin (green), and the merged image is shown along with a close-up.

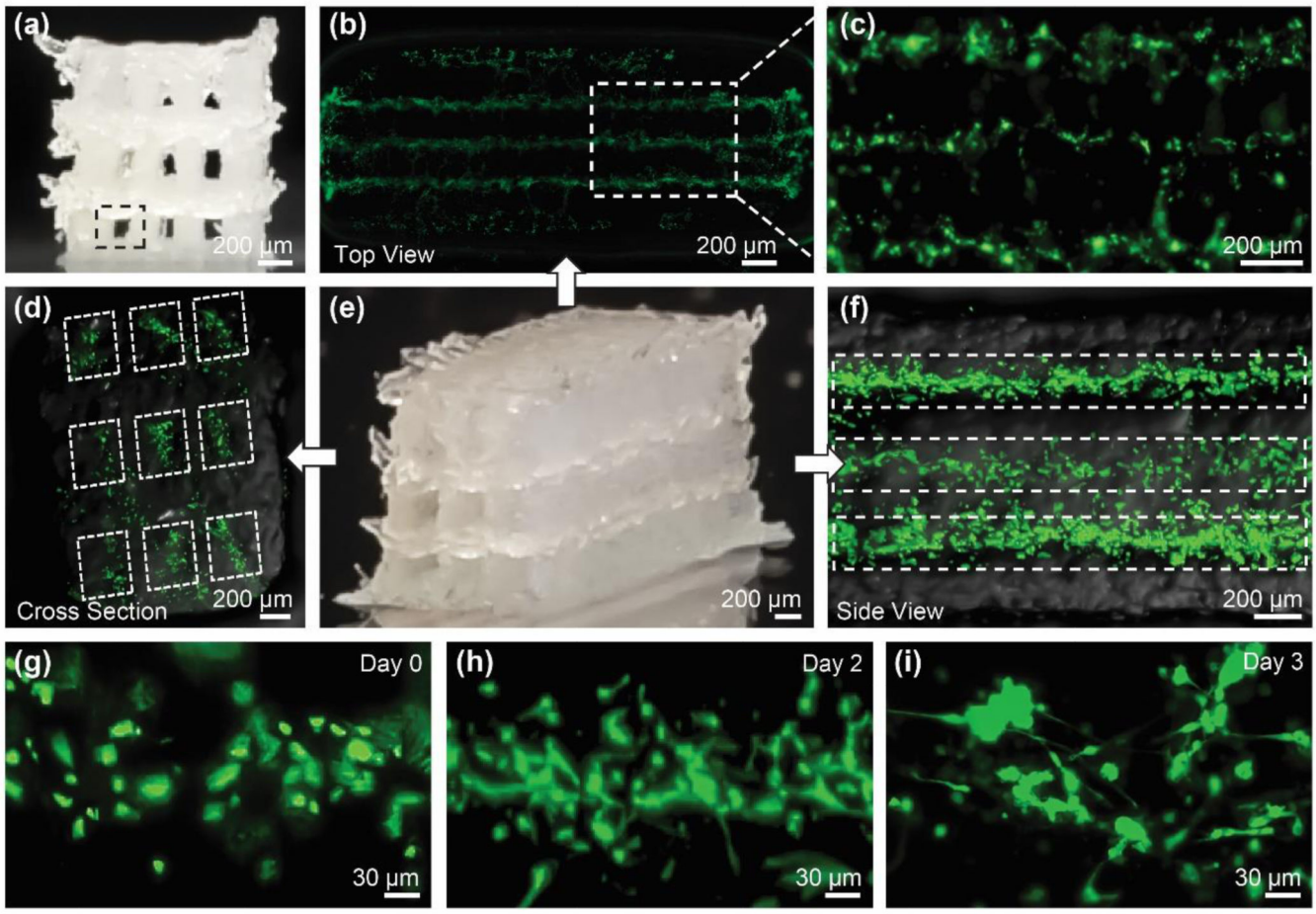

Figure 4.

Construction of neurocompatible 3D alginate-based scaffolds. (a) Cross-sectional view of the AG/MC scaffold showing ~150 μm channel resolution. (b)-(e) Scaffolds were fabricated and cells were alive for 3 days after printing in all three layers. (b),(c) Top-down, (d) Cross-sectional, and (f) Longitudinal side view of fluorescence images of a 3D printed scaffold. (g)-(i) Time progression of sNPCs in an AG/MC scaffold showing processes elongating over a period of 3 days in culture.

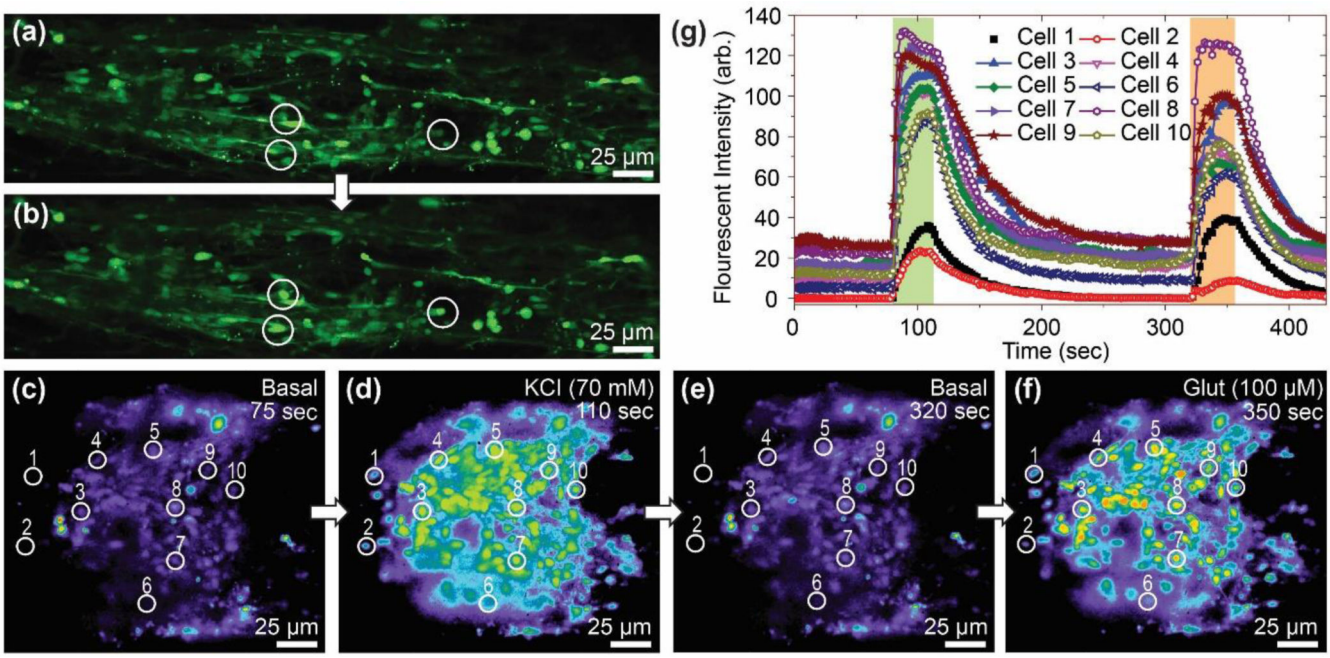

Figure 5.

Functional characterization of 3D bioprinted sNPCs via calcium imaging. (a,b) Video-captured sequence of the calcium imaging of sNPCs bioprinted in a silicone scaffold with long axon projections 14 days after printing. High-resolution confocal imaging shows cell bodies and adjacent axons with calcium transients. (c-f) Video-captured sequence of the calcium imaging of sNPCs bioprinted in a silicone scaffold. Cells in the scaffold before and after (c,d) 70 mM potassium chloride (KCl), and (e,f) 100 μM glutamate were added. (g) Time-dependent fluorescent intensity of 10 cells marked in (c-f). Fluorescent intensity was measured after the addition of high KCl and the neurotransmitter glutamate.